Rare Metal Materials and Engineering
Volume 51, Issue 7, July 2022
Available online at www.rmme.ac.cn

Science Press

Cite this article as: Zou Youchun, Xiong Chao, Yin Junhui, et al. Anti-penetration Performance and Micro-damage Mechanism of Ti-6Al-4V Alloy Composite Armor[J]. Rare Metal Materials and Engineering, 2022, 51(07): 2329-2335.

ARTICLE

Anti-penetration Performance and Micro-damage Mechanism of Ti-6Al-4V Alloy Composite Armor

Zou Youchun[1], Xiong Chao[1], Yin Junhui[1], Deng Huiyong[1], Cui Kaibo[1], Zhang Sa[1], An Zhiguo[2], Bai Lijuan[2]

[1] Department of Artillery Engineering, Army Engineering University of PLA, Shijiazhuang 050003, China; [2] Physical and Chemical Test Center, HBIS Group Research Institute, Shijiazhuang 050003, China

Abstract: In order to study the optimal combination of Ti-6Al-4V (TC4) alloy with silicon carbide (SiC) ceramics and ultra-high molecular weight polyethylene (UHMWPE) in composite armor, the penetration resistance and macro-damage of the complex material with composite structure of SiC/UHMWPE/TC4 (I) and SiC/TC4/UHMWPE (II) were analyzed, and the micro-damage of TC4 alloy was also discussed. Results show that the bullet hole edges of TC4 alloy in composite structure I are relatively smooth without cracks, and there are a few adiabatic shear bands (ASBs) propagated along the straight lines. The bullet hole edges of TC4 alloy in composite structure II are rough, and there are cracks and spalling damage. There are many curved and bifurcated ASBs in composite structure II. The penetration process of TC4 alloy in composite structure II includes the pit opening stage, stable penetration stage, and perforation stage. The adiabatic shear behavior of TC4 alloy in composite structure II is more complicated than that in composite structure I, resulting in more energy consumption. In addition, the tensile failure caused by UHMWPE in the composite structure II is also one of characteristics of the high energy consumption failure mode. Therefore, the SiC/TC4/UHMWPE composite structure can efficiently exert the energy consumption mechanisms of TC4 alloy and UHMWPE, and the anti-penetration performance of the complex armor with this composite structure is better than that with the composite structure I.

Key words: Ti-6Al-4V alloy; anti-penetration performance; composite armor; adiabatic shear band

Titanium alloy has the characteristics of low density, high strength, excellent fatigue strength, good crack growth resistance, low temperature toughness, and fine corrosion resistance, and therefore attracts wide attention in the aerospace and ship fields. The titanium alloy is lightweight and has excellent ballistic resistance, resulting in the common use in the field of military protection[1,2].

Titanium alloy exhibits a local plastic deformation and instability phenomenon under high-speed loading, namely the adiabatic shear phenomenon[3-5]. The narrow band-shaped area caused by shear deformation is named as adiabatic shear band (ASB). The adiabatic shear is a unique local instability phenomenon of materials, which is closely related to the material failure[6-8]. In order to improve the anti-penetration performance of titanium alloys, it is necessary to explore the damage behavior under impact load. The researches on the microstructure and damage law of titanium alloys under the projectile penetration provide the theoretical basis for the application of titanium alloy in protective armor[9-11].

Zheng et al[12] studied the relationship between the damage mechanism and microstructure characteristics of Ti-6Al-4V (TC4) alloy against armor-piercing projectiles of 12.7 mm in diameter. It is found that the regularly spaced propagation features of ASBs facilitate the failure mechanism of ductile hole enlargement in the equiaxed microstructure; the net-like propagation features of ASBs facilitate the failure mechanism of brittle fragmentation in the lamellar microstructure. Sukumar et al[13] studied the performance of β-CEZ titanium alloys with different microstructures against the armor-piercing projectiles of 7.62 mm in diameter. It is found that compared with that of TC4 alloys, the penetration resistance of β-CEZ titanium alloys is not significantly improved, but the

Received date: July 14, 2021
Foundation item: Military Key Task Project of China (MS201507A0132)
Corresponding author: Xiong Chao, Ph. D., Professor, Department of Artillery Engineering, Army Engineering University of PLA, Shijiazhuang 050003, P. R. China, E-mail: ljgcdxxiongchao@163.com

β-CEZ titanium alloys present more ASBs and cracks. Li et al[14] compared the microstructure and anti-penetration properties of Ti684 alloy and TC4 alloy, and demonstrated that Ti684 alloy can generate stress-induced martensite during the penetration process, which delays the ASBs formation, thereby presenting better anti-penetration properties. Yang et al[15] found that the anti-penetration performance of TC21 alloy is similar to that of TC4 alloy, and both alloys are prone to adiabatic shear failure.

Most researches focus on the anti-penetration and microstructure of individual titanium alloys[16-18], but those of complex material with composite protective structures are rarely investigated. At present, TC4 alloy is usually combined with ceramics and fiber composite materials to form a composite armor, which shows better anti-penetration performance than the alloy with homogeneous structure does and is widely used in the field of military protection[19,20]. Thus, in this research, the complex materials with composite structures were investigated. The penetration tests for the complex materials with composite protective structures were conducted. Firstly, the anti-penetration performance of the complex materials of composite structures was evaluated. Subsequently, the macroscopic failure mechanisms were analyzed, and the influence of the component arrangement on the anti-penetration performance was studied. Finally, the failure mechanisms of TC4 alloy were studied from the microstructure perspective, and the influence of failure mechanisms of TC4 alloy on the anti-penetration performance of the complex material of composite structures was analyzed.

1 Experiment

This research used the composite armor consisting of ceramics (SiC), metals (TC4 alloy), and fiber composite materials (ultra-high molecular weight polyethylene, UHMWPE). According to the characteristics of different materials, two composite structures were designed: the composite structure I of SiC/UHMWPE/TC4 and the composite structure II of SiC/TC4/UHMWPE. The anti-penetration performance of the complex material with these two composite structures was evaluated.

The thickness of SiC, UHMWPE, and TC4 alloy was 5, 5, and 6 mm, respectively. The cross-section size of specimen with each composite structure was 150 mm×150 mm, and the interfaces between the layers were bonded by epoxy resin. TC4 alloy has the equiaxed microstructure, which is mainly composed of equiaxed or short rod-shaped α grains and β phases distributed in the gaps of α grains. The transition temperature of β phase is 993±5 °C, and its chemical composition is 6.42Al-4.17V-0.19Fe-0.20O-0.01C-0.02N-0.003H-Ti (wt%). The equiaxed microstructure was obtained in the α+β region through the solution treatment at 950 °C for 1 h followed by furnace cooling.

The schematic diagram of penetration test device is shown in Fig. 1. The ballistic rifle was used to shoot the armor-piercing projectiles of 14.5 mm in diameter, and the velocity measuring device was used to measure the initial velocity of the projectile. The 603 armor steel of 45 mm in thickness was placed behind the target, and the anti-penetration performance of the complex material with composite structures was evaluated through the residual penetration depth of 603 armor steel. The complex materials with each composite structure were tested 3 times, and the average value of residual penetration depth was used to reduce the error. The penetrated TC4 alloy was cut along the center line of the crater for macroscopic and microscopic damage analyses. The specimens were ground, polished, and etched via the solution of 2 mL HF+6 mL HNO_3+92 mL H_2O for 10~15 s, and then examined by Axiovert-2000MAT optical microscope (OM) and ZEISS Sigma 500 scanning electron microscope (SEM) for microstructure analysis.

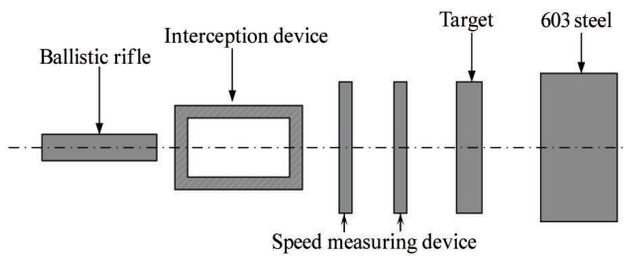

Fig.1 Schematic diagram of penetration test device

2 Results and Discussion

2.1 Anti-penetration performance

The mass efficiency F_m and thickness efficiency F_s of the complex materials of composite structures are calculated by the residual penetration depth P_{res} and reference penetration depth P_{ref} of the 603 armor steel. The F_m and F_s calculation formulae[20] are expressed, as follows:

$$F_m = \frac{(P_{ref} - P_{res})\rho_{603}}{\delta\rho_{hs}} \quad (1)$$

$$F_s = \frac{P_{ref} - P_{res}}{\delta} \quad (2)$$

where P_{ref} is the depth of penetration of the bare 603 armor steel, P_{res} is the residual depth of penetration of 603 armor steel behind the complex material of composite structure, ρ_{603} is the density of 603 armor steel, δ is the thickness of the complex material, and ρ_{hs} is the average density of the complex material. ρ_{603} is 7.86 g/cm^3, and abundant test data prove that P_{ref} of 603 steel is 43 mm. As shown in Fig.2, the 603 armor steel is placed behind the complex materials of composite structure.

The calculation results are shown in Table 1. The residual penetration depth of the complex materials of composite structures I and II is 14.51 and 7.17 mm, respectively. The mass efficiency and thickness efficiency of complex materials of composite structure I and II are all greater than 1, indicating that the designed composite structures have advantages in reduction of mass and thickness, and the penetration resistance of complex material of composite structure II is better than that of composite structure I.

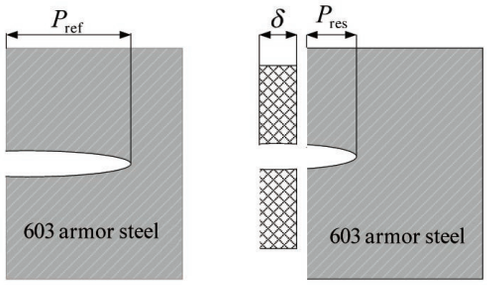

Fig.2 Schematic diagram of anti-penetration evaluation through depth of penetration method

Table 1 Mass efficiency F_m and thickness efficiency F_s of complex materials of different composite structures

Composite structure	ρ_{hs}/g·cm^{-3}	δ/mm	P_{res}/mm	F_m	F_s
I	2.756	17.4	14.51	4.67	1.64
II	2.642	18.3	7.17	5.82	1.96

2.2 Macro-damage features

The appearances of penetrated UHMWPE are shown in Fig. 3. It can be seen that UHMWPE in complex materials of composite structure I and composite structure II fails due to the shear failure and tensile failure, respectively. As for the composite structure I, TC4 alloy has a constraint on UHMWPE, resulting in small deformation and shear failure of UHMWPE. The UHMWPE in complex materials of composite structure II is placed in back position and has sufficient deformation space. The velocity of the projectile after penetration of TC4 alloy is low, and UHMWPE undergoes tensile failure during the projectile penetration. The fiber composite materials mainly rely on stretching and deformation of fibers to consume energy, and the shear failure cannot fully exert its energy consumption mechanism in this case.

The appearances of perforated channels of TC4 alloy are shown in Fig. 4. The bullet hole of complex material of composite structure I is relatively smooth, and the damage mode is brittle fragmentation. The bullet hole of complex material of composite structure II is rough, there are obvious

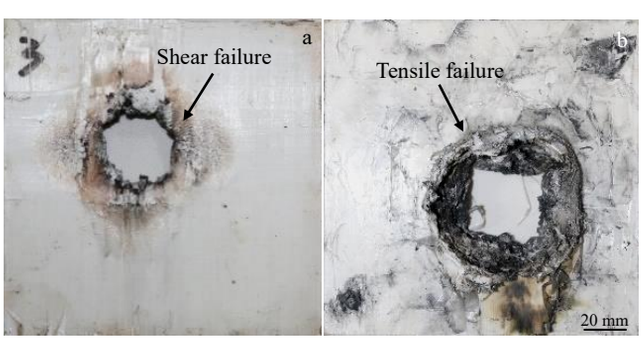

Fig.3 Appearances of penetrated UHMWPE in complex materials of composite structure I (a) and composite structure II (b)

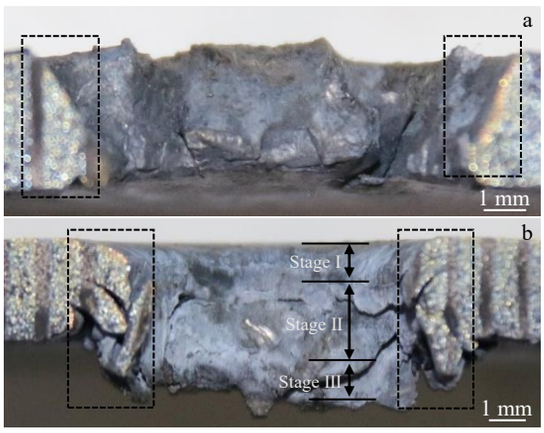

Fig.4 Appearances of perforated channels of TC4 alloy in complex materials of composite structure I (a) and composite structure II (b)

fragments on the back, and the damage mode is spalling damage. The brittle fragmentation and spalling damage of TC4 alloy belong to the damage modes of low energy consumption and high energy consumption, respectively. Therefore, the composite structure II can fully exert the energy dissipation mechanism of UHMWPE and TC4 alloy, and its anti-penetration performance is better than that of the composite structure I.

2.3 Micro-damage features of TC4 alloy

TC4 alloy suffers the high temperature, high pressure, and high strain rate during the process of projectile penetration. Due to the extremely short penetration duration, the heat generated inside TC4 alloy cannot be completely dissipated, leading to adiabatic phenomenon. The adiabatic phenomenon leads to the instability of the material, and the severe plastic deformation occurs at local locations, forming ASBs[21]. As shown in Fig. 5, the morphology of ASB is different from that of the matrix. The microstructure of ASB is broken due to the shearing deformation, and there is a clear boundary with the matrix, as indicated by the arrows in Fig. 5. The stress and strain concentrations tend to occur in ASB. When the temperature reaches a certain level, the material strength decreases, the deformation increases, and the deformation of ASB and matrix is not coordinated. This uneven deformation leads to the formation of microcracks and micro-voids.

The sampling positions are shown in the dashed rectangles in Fig. 4a, and the corresponding microstructure of TC4 alloy in the complex material of composite structure I is shown in Fig. 6. The bullet hole edges of TC4 alloy in complex material of composite structure I are relatively smooth. The magnified microstructures at position A, B, C, and D in Fig. 6 are shown in Fig. 7. The number of ASBs is small, and ASBs are propagated along the straight lines, as indicated by the arrows in Fig. 7. No cracks can be observed in ASBs.

The sampling positions are shown in the dashed rectangles in Fig. 4b, and the corresponding microstructure of TC4 alloy in complex material of composite structure II is shown in

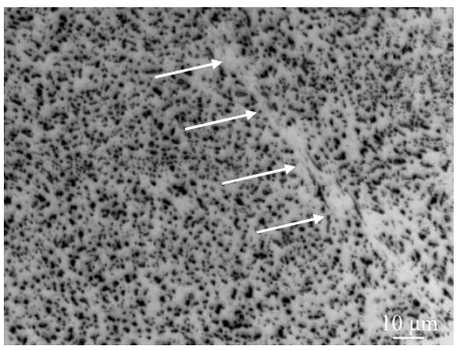

Fig.5 Morphology of ASB

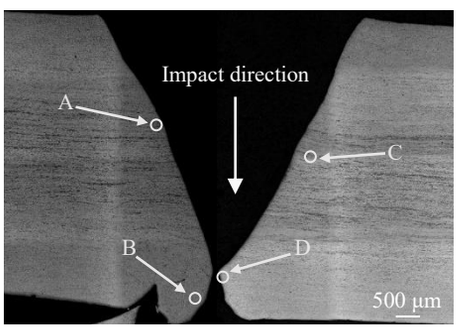

Fig.6 Microstructure of TC4 alloy in complex material of composite structure I

Fig. 8. The bullet holes of TC4 alloy have rough edges and cracks, and the spalling damage appears on the back. The magnified microstructures at position A, B, C, and D in Fig. 8 are shown in Fig. 9. As shown in Fig. 9a, due to the inconsistent deformation of ASB and matrix, the microcrack sources appear in ASB. The penetration process involves the complex stress wave propagation, and the reflected stress wave σ_R is expressed by Eq.(3)[22], as follows:

$$\sigma_R = \frac{\rho_2 c_2 - \rho_1 c_1}{\rho_1 c_1 + \rho_2 c_2} \sigma_I \quad (3)$$

where σ_I is the incident stress wave; ρ_1 and ρ_2 are the densities of TC4 alloy and UHMWPE, respectively; c_1 and c_2 are the stress wave speeds of TC4 alloy and UHMWPE, respectively; When σ_R is less than 0, the reflected wave is a tensile stress wave.

Since the wave impedance of TC4 alloy is greater than that of UHMWPE, based on Eq.(3), it can be found that when the stress wave is propagated from TC4 alloy to UHMWPE, part of the stress wave is reflected to form a tensile stress wave. The microcrack sources of ASBs form the macroscopic cracks under the action of tensile stress wave, and the damage is more severe.

The microcracks are initiated, expand, and merge along ASB, and form macro-cracks under the combined actions of tensile stress and shear stress. Eventually, TC4 alloy forms the fragments and separates at the cracks, resulting in target damage. As shown in Fig. 9b~9d, many ASBs, curved propagation (indicated by the arrows in Fig.9), and bifurcation phenomena can be observed, which provide more locations and paths for the crack sources. The initiation, expansion, and merging of ASBs and cracks consume a lot of energy. Therefore, TC4 alloy in the complex material of composite structure II consumes more energy than that of composite structure I does.

The damage behavior of TC4 alloy in complex material of composite structure II is more complicated, and the following discussion is all about the cases of composite structure II. As

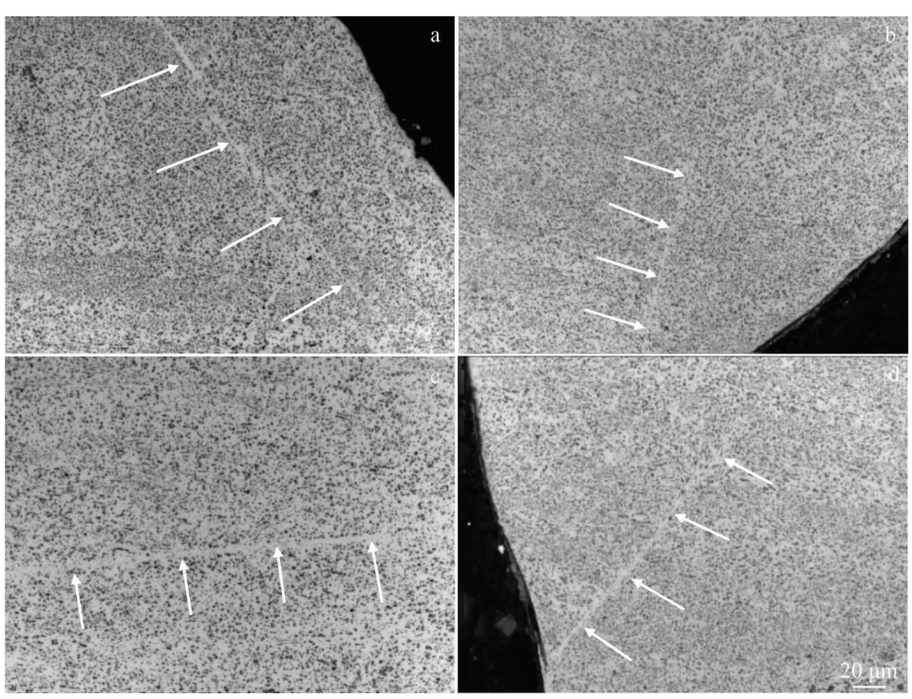

Fig.7 Magnified microstructures of ASBs at position A (a), position B (b), position C (c), and position D (d) in Fig.6

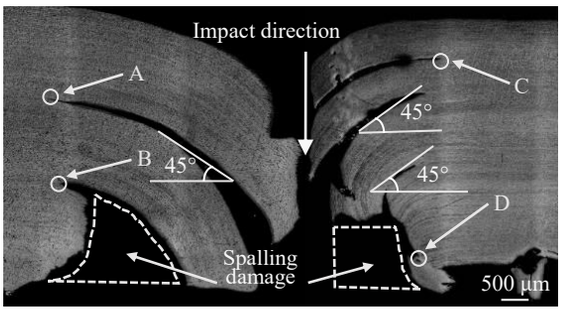

Fig.8 Microstructure of TC4 alloy in complex material of composite structure II

shown in Fig. 4b, the process of projectile penetration into TC4 alloy can be clearly divided into three stages: Stage I-pit opening stage; Stage II -stable penetration stage; Stage III - perforation stage.

In the pit opening stage, the projectile speed is the fastest, and the force between the projectile and the TC4 alloy is also the largest, which is much greater than the dynamic fracture strength of the TC4 alloy. Therefore, TC4 alloy preferentially fails in the form of avalanche. Fig. 10a shows the fracture morphology of TC4 alloy in the pit opening stage. There are many tearing edges, which agrees with the avalanche features. In the pit opening stage, the heat generated by the interaction between the projectile and the TC4 alloy does not reach the temperature for ASB generation. Therefore, as shown in Fig. 10c, the TC4 alloy only undergoes the grain elongation without ASBs. In addition, the temperature cannot either reach the melting temperature of the projectile. As shown in Fig.10b, EDS spectrum of the pit opening position shows that the composition is basically the same as that of the matrix, and there is no element from the projectile, suggesting that there is no melting phenomenon of the projectile.

In the stable penetration stage, there is a significant

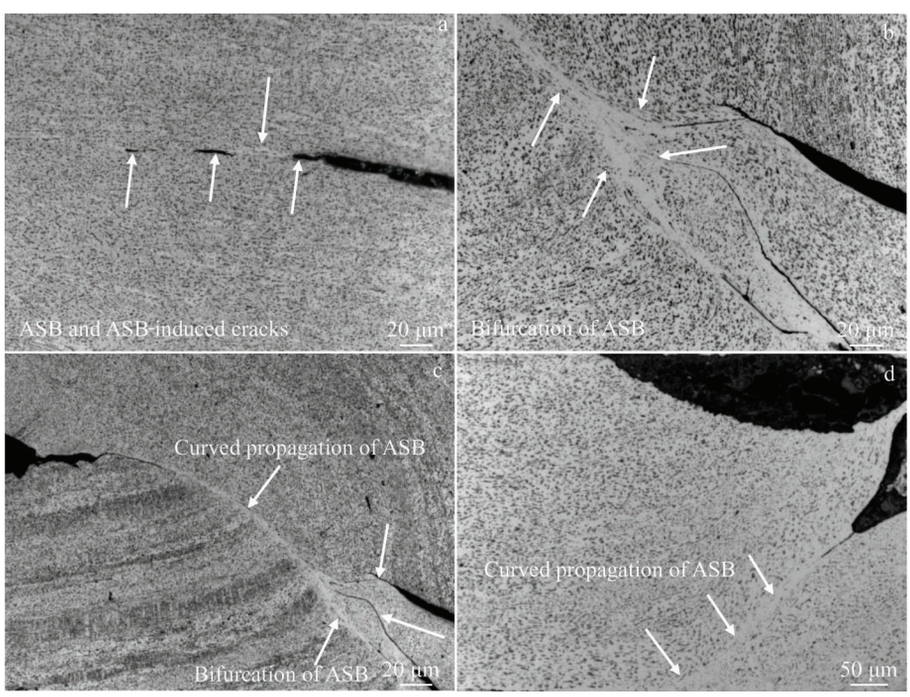

Fig.9 Magnified microstructures of ASBs at position A (a), position B (b), position C (c), and position D (d) in Fig.8

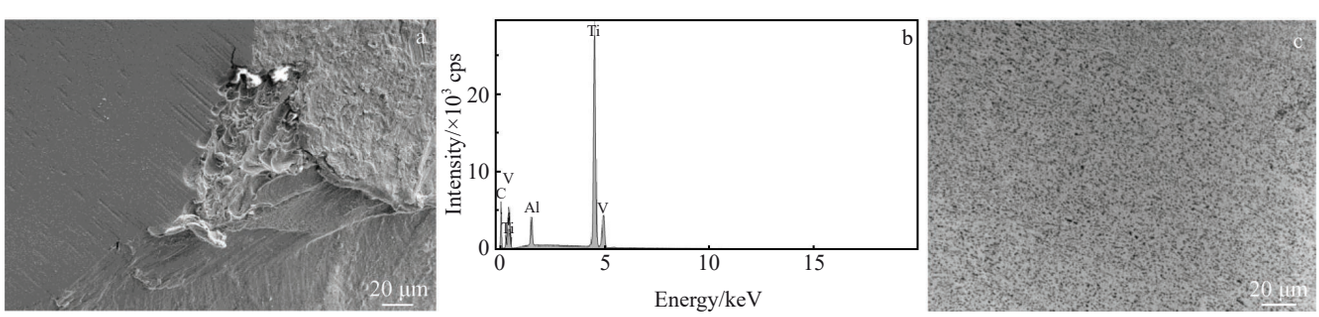

Fig.10 Fracture morphology (a) and EDS spectrum (b) of TC4 alloys in composite structure II in pit opening stage; microstructure of TC4 alloy in composite structure II suffering grain elongation without ASBs (c)

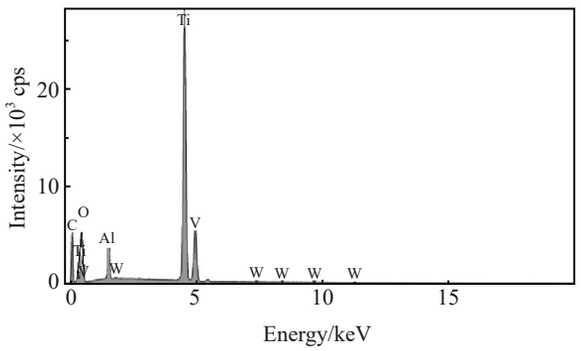

Fig.11 EDS spectrum of TC4 alloy of composite structure II in perforation stage

accumulation of metal around the crater, and TC4 alloy cannot consume the kinetic energy of the projectile in the form of avalanche. Therefore, a stable state of high temperature, high pressure, and high strain rate is established between the projectile and the TC4 alloy, namely the adiabatic phenomenon. At high temperature, the strength of TC4 alloy decreases and the softening effect is obvious. Under the action of shearing force, the adiabatic shear failure and strong plastic deformation are extremely easy to occur, causing serious damage to the TC4 alloy. As shown in Fig.8, since TC4 alloy is subjected to the greatest shear stress along the direction with an angle of 45° to the penetration direction, ASBs and cracks are initiated significantly easily. With the further expansion of the shear zone, the shear angular strain of the TC4 alloy is increased, and the shear localization is fully formed, which is characterized by the bifurcation, expansion, and increasing number of ASBs.

The projectile energy is largely dissipated in Stage I and Stage II, resulting in the fact that the grain deformation is very small in the perforation stage. As shown in Fig. 11, EDS spectrum of TC4 alloy in Stage III shows that the alloy composition contains tungsten, indicating that the damage of projectile is serious in the perforation stage.

3 Conclusions

1) In the SiC/ultra-high molecular weight polyethylene (UHMWPE)/Ti-6Al-4V (TC4) composite structure, TC4 alloy suffers brittle fragmentation, and UHMWPE suffers shear failure. In the SiC/TC4/UHMWPE composite structure, the TC4 alloy suffers spalling damage, and UHMWPE suffers the tensile failure. The spalling damage of TC4 alloy and the tensile failure of UHMWPE belong to the failure mechanism of high energy consumption. The structural form of the SiC/TC4/UHMWPE composite structure fully exert the energy dissipation mechanism of TC4 alloy and UHMWPE, and the complex material with this composite structure shows better anti-penetration performance.

2) The microstructure of TC4 alloy in complex materials of SiC/UHMWPE/TC4 composite structure shows that the edges of bullet holes are relatively smooth, the number of adiabatic shear bands (ASBs) is small, and ASBs are straightly propagated without cracks, which promotes the brittle fragmentation of TC4 alloy. The microstructure of the TC4 alloy in complex material of SiC/TC4/UHMWPE composite structure shows that the edges of the bullet holes are rough, the number of ASBs is large, and the ASBs are bent and bifurcated. ASBs and microcracks can form the macro-cracks under the action of tensile stress wave, which promotes the spalling damage of the TC4 alloy. The initiation, expansion, and merging of ASBs and cracks cause TC4 alloy in SiC/TC4/UHMWPE composite structure to consume more energy.

3) In the pit opening stage, the kinetic energy of the projectile is mainly consumed by the damage mechanism of avalanche. In the stable penetration stage, the kinetic energy of the projectile is mainly consumed by the damage mechanism of adiabatic shear, cracks, and plastic deformation. In the perforation stage, the kinetic energy of the projectile is mainly consumed by the damage mechanism of plastic deformation, and the projectile is seriously damaged.

References

1 Walters W, Gooch W, Burkins M. *International Journal of Impact Engineering*[J], 2001, 26(1-10): 823
2 Gooch W A, Burkins M S, Walters W P *et al. International Journal of Impact Engineering*[J], 2001, 26(1-10): 243
3 Xin Y P, Zhu Z S, Wang X N *et al. Rare Metal Materials and Engineering*[J], 2020, 49(10): 3361
4 Huang Bin, Ren Weijia, Zhang Yanmei *et al. Rare Metal Materials and Engineering*[J], 2018, 47(9): 2705 (in Chinese)
5 Peng Meiqi, Cheng Xingwang, Zheng Chao *et al. Rare Metal Materials and Engineering*[J], 2017, 46(8): 2227 (in Chinese)
6 Meyer L W, Staskewitsch E, Burblies A. *Mechanics of Materials* [J], 1994, 17(2-3): 203
7 Murr L E, Ramirez A C, Gaytan S M *et al. Materials Science and Engineering A*[J], 2009, 516(1-2): 205
8 Yang Y, Li X M, Tong X L *et al. Materials Science and Engineering A*[J], 2011, 528(7-8): 3130
9 Yang Shen, Guan Qingfeng. *Rare Metal Materials and Engineering*[J], 2016, 45(9): 2307 (in Chinese)
10 Li Mingbing, Wang Xinnan, Shang Guoqiang *et al. The Chinese Journal of Nonferrous Metals*[J], 2021, 31(2): 365 (in Chinese)
11 Huang Junhao, Wang Lin, Liu Xiaopin *et al. Acta Armamentarii* [J], 2021, 42(1): 124 (in Chinese)
12 Zheng C, Wang F C, Cheng X W *et al. International Journal of Impact Engineering*[J], 2015, 85: 161
13 Sukumar G, Singh B B, Bhattacharjee A *et al. International Journal of Impact Engineering*[J], 2013, 54: 149
14 Li Rongting, Fan Qunbo, Wang Fuchi *et al. Rare Metal Materials and Engineering*[J], 2015, 44(8): 1937 (in Chinese)
15 Yang Kaiwen, Cheng Xingwang, Zheng Chao *et al. Rare Metal Materials and Engineering*[J], 2015, 44(11): 2728 (in Chinese)
16 Zheng C, Wang F C, Cheng X W *et al. Materials Science and*

Engineering A[J], 2014, 608: 53
17 Sun K, Yu X D, Tan C W *et al. Materials Science and Engineering A*[J], 2014, 595: 247
18 Sun K, Yu X D, Tan C W *et al. Materials Science and Engineering A*[J], 2014, 606: 257
19 Nassir N A, Birch R S, Cantwell W J *et al*. *Composite Structures* [J], 2020, 245: 112 398
20 An X Y, Tian C, Sun Q T *et al. Defence Technology*[J], 2020, 16(1): 77
21 Huang B, Miao X F, Luo X *et al*. *Materials Characterization*[J], 2019, 151: 151
22 Jin Jiefang, Wang Jie, Guo Zhongqun *et al*. *Journal of China Coal Society*[J], 2019, 44(2): 435 (in Chinese)

Ti-6Al-4V合金复合装甲的抗侵彻性能及微观损伤机理

邹有纯[1]，熊　超[1]，殷军辉[1]，邓辉咏[1]，崔凯波[1]，张　飒[1]，安治国[2]，白丽娟[2]
(1. 中国人民解放军陆军工程大学 火炮工程系，河北 石家庄 050003)
(2. 河钢集团钢研总院 理化检测中心，河北 石家庄 050003)

摘　要：为研究复合装甲中Ti-6Al-4V（TC4）合金与碳化硅陶瓷和超高分子量聚乙烯（UHMWPE）的最佳组合形式，分析了2种复合结构SiC/UHMWPE/TC4（I）和SiC/TC4/UHMWPE（II）的抗侵彻性能和宏观损伤以及TC4合金的微观损伤。结果表明：复合结构I中TC4合金的微观组织表现为弹孔边缘较为平滑，没有出现裂纹，绝热剪切带（ASB）数量较少，并且为直线传播；复合结构II中TC4合金微观组织表现为弹孔边缘粗糙，存在裂纹，背部存在崩落损伤，ASB数量多，并且呈弯曲和分叉现象。TC4合金在复合结构II中的侵彻过程分为开坑阶段、稳定侵彻阶段和穿孔阶段。复合结构II中TC4合金的绝热剪切行为更为复杂，导致耗能更多。此外，复合结构II中UHMWPE产生拉伸破坏也属于高耗能失效机制。因此，SiC/TC4/UHMWPE复合结构能够充分发挥TC4和UHMWPE的高耗能机制，抗侵彻性能好于复合结构I。

关键词：Ti-6Al-4V合金；抗侵彻性能；复合装甲；绝热剪切带

作者简介：邹有纯，男，1997年生，硕士，中国人民解放军陆军工程大学火炮工程系，河北 石家庄 050003，E-mail：zouyouchun2019@163.com